Northumbria Research Link

UniversityLibrary

Rigid Foldability of Generalized Triangle Twist Origami Pattern and Its Derived 6*R* Linkages

Huijuan Feng, first author
a. School of Mechanical Engineering, Tianjin University, Tianjin 300072, PR China
b. Université Clermont Auvergne, CNRS, SIGMA Clermont, Institut Pascal, F-63000 Clermont-Ferrand, France
School of Mechanical Engineering, Tianjin University, No.135 Yaguan Road, Jinnan District, Tianjin 300350, P. R. China.
huijuan@tju.edu.cn

Rui Peng, second author
a. School of Mechanical Engineering, Tianjin University, Tianjin 300072, PR China
School of Mechanical Engineering, Tianjin University, No.135 Yaguan Road, Jinnan District, Tianjin 300350, P. R. China.
pengrui@tju.edu.cn

Jiayao Ma, third author
a. School of Mechanical Engineering, Tianjin University, Tianjin 300072, PR China
c. Key Laboratory of Mechanism Theory and Equipment Design of Ministry of Education, Tianjin University, Tianjin 300072, PR China
School of Mechanical Engineering, Tianjin University, No.135 Yaguan Road, Jinnan District, Tianjin 300350, P. R. China.
jiayao.ma@tju.edu.cn

Yan Chen, corresponding author
a. School of Mechanical Engineering, Tianjin University, Tianjin 300072, PR China
c. Key Laboratory of Mechanism Theory and Equipment Design of Ministry of Education, Tianjin University, Tianjin 300072, PR China
School of Mechanical Engineering, Tianjin University, No.135 Yaguan Road, Jinnan District, Tianjin 300350, P. R. China.
yan_chen@tju.edu.cn
ASME Member

ABSTRACT

Rigid origami is a restrictive form of origami that permits continuous motion between folded and unfolded states along the pre-determined creases without stretching or bending of the facets. It has great potential in engineering applications, such as foldable structures that consist of rigid materials. The rigid foldability is an important characteristic of an origami pattern, which is determined by both the geometrical parameters and the mountain-valley crease (M-V) assignments. In this paper, we present a systematic method to analyze the rigid foldability and motion of the generalized triangle twist origami pattern using the kinematic equivalence between the rigid origami and spherical linkages. All schemes of M-V assignment are derived based on the flat-foldable conditions, among which rigidly foldable ones are identified. Moreover, a new type of overconstrained 6R linkage and a variation of doubly collapsible octahedral Bricard are developed by applying kirigami technique to the rigidly foldable pattern without changing its degree of freedom. The proposed method opens up a new way to generate spatial overconstrained linkages from the network of spherical linkages. It can be readily extended to other types of origami patterns.

1. INTRODUCTION

Origami, an art of intricately folding a 2D flat sheet of paper into elaborate 3D sculptures and objects, has drawn increasing attention from engineers recently. Many of its techniques can be used in the design of foldable structures due to its superior efficiency of packaging large surface structures into smaller volumes for storage or transportation. Since most materials used in the structures, e.g., solar arrays [1, 2] and satellite antenna reflectors [3] in aerospace engineering, mobile facets [4, 5] and

reconfigurable and multi-locomotive devices [6, 7] in civil engineering, and stent grafts [8] and miniature origami robots [9, 10, 11] in biomedical engineering, are relatively rigid in comparison with paper, particular attention has been drawn to rigid origami. It is a restrictive form of origami, where continuous folding motions are generated by its facets rotating around pre-determined creases without being stretched or bent.

To achieve rigid foldability, motions around each vertex must be compatible with those around its neighbors, attained only under specific pattern geometries. Recent work shows that both the geometrical conditions and mountain-valley crease (M-V) assignments affect the rigid foldability of origami patterns [12]. Numerical algorithms [13], quaternions and dual quaternions [14], matrix methods [15] have been proposed to judge the rigid foldability of origami patterns. From the mechanism perspective, the creases of rigid origami can be treated as rotation joints and the paper facets treated as links [16]. The creases intersect at one vertex is kinematically a spherical linkage [17]. Then the crease pattern can be modeled as a network of spherical linkages, and its rigid foldability can be analyzed by the kinematic approach.

Inspired by rigid origami, several novel mechanisms have been developed. For instance, two integrated planar-spherical overconstrained mechanisms were proposed from origami cartons with crash-lock bases [18]. A parallel mechanism with three-spherical kinematic chains has been designed based on a waterbomb origami pattern [19], of which the reaction force was analyzed based on the repelling-screw [20]. Furthermore, this origami parallel mechanism has been used to design an extensible continuum robot [21] and an origami grasper for minimally invasive surgery [22].

Recently, several novel mobile assemblies of Bennett linkages have been derived from the flat-foldable four-crease origami patterns by taking the thick-panel form of an origami pattern as an intermediate bridge [23]. In addition, a novel 8*R* linkage which can evolve into overconstrained 6*R* linkages has been proposed from a kirigami pattern with eight creases [24].

On the other hand, origami twists like the square twist, the triangle twist, and the hexagon twist, are often used for tessellation of origami patterns in art [25]. Among them, the triangle twist origami pattern is formed by a central triangle plus four-crease vertices extended from each side of the triangle. It has been proved that no triangle twist origami pattern with parallel pleats is rigidly foldable [12]. However, it did not tackle the rigid foldability of triangle twist origami patterns with non-parallel pleats. Here we are going to make a thorough analysis on rigid foldability and motion of the generalized triangle twist origami pattern concerning all position relation of pleats and all schemes of M-V assignment. Meanwhile, the kirigami technique will be applied for the generation of new 6*R* linkages from the rigidly foldable triangle twist patterns.

The layout of this paper is as follows. The kinematics and rigid foldability of a typical generalized triangle twist origami pattern are presented in section 2. Section 3 gives all schemes of M-V assignment for the generalized triangle twist origami pattern and discusses their effect on rigid foldability. The type of the derived 6*R* linkage from the triangle twist kirigami pattern is identified and a new kind of overconstrained 6*R* linkage is proposed in section 4. The final part is the conclusion in section 5 which ends the paper.

2. RIGID FOLDABILITY OF THE GENERALIZED TRIANGLE TWIST ORIGAMI PATTERN

In the origami art, a triangle twist is a crease pattern consisting of an equilateral triangle with parallel pleats radiating from its three sides [26], see Fig. 1(a). If we change the central equilateral triangle to a general one and remove the parallel constraint on the pleats, a generalized triangle twist as shown in Fig. 1(b) would be formed. The kinematics of the four-crease rigid origami vertex is studied firstly in order to analyze rigid foldability of the generalized triangle twist origami pattern.
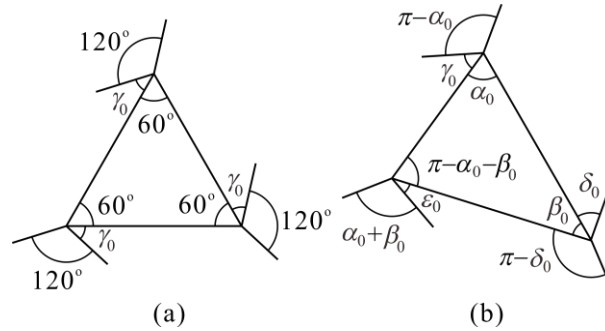
Fig. 1   (a) An art triangle twist, (b) a generalized triangle twist, where α_0, β_0, γ_0, δ_0 and ε_0 is arbitrary within the domain $(0, \pi)$ and $\alpha_0 + \beta_0 \in (0, \pi)$.

The Denavit-Hartenberg (D-H) notation of adjacent links connected by revolute joints [27] is presented in Fig. 2, where the axis z_i is along the revolute joint i, the axis x_i is the common normal from z_{i-1} to z_i, $a_{i(i+1)}$ is the normal distance between z_i and z_{i+1}, $\alpha_{i(i+1)}$ is the angle of rotation from z_i to z_{i+1}, positive along the axis x_{i+1}, R_i is the normal distance between x_i and x_{i+1}, positive along the axis z_i, and θ_i is the angle of

rotation from x_i to x_{i+1}, positive along the axis z_i. Using the matrix method for kinematics analysis, the closure equation for a single loop linkage consisting of n links is

$$T_{21} \cdot T_{32} \cdots T_{n(n-1)} \cdot T_{1n} = I_4, \qquad (1)$$

where the transformation matrix $T_{(i+1)i}$ is

$$T_{(i+1)i} = \begin{bmatrix} \cos\theta_i & -\cos\alpha_{i(i+1)}\sin\theta_i & \sin\alpha_{i(i+1)}\sin\theta_i & a_{i(i+1)}\cos\theta_i \\ \sin\theta_i & \cos\alpha_{i(i+1)}\cos\theta_i & -\sin\alpha_{i(i+1)}\cos\theta_i & a_{i(i+1)}\sin\theta_i \\ 0 & \sin\alpha_{i(i+1)} & \cos\alpha_{i(i+1)} & R_i \\ 0 & 0 & 0 & 1 \end{bmatrix}, \qquad (2)$$

which transforms the expression in the $(i+1)$ th coordinate system to the i th coordinate system, and when $i+1 > n$, it is replaced by 1.
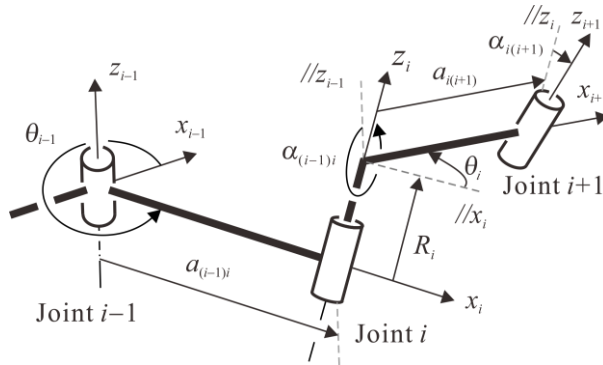

Fig. 2 The D-H notation of adjacent links connected by revolute joints

As for a spherical 4R linkage, the axes intersect at one point as shown in Fig. 3, which means the lengths and offsets of all links are zero and thus Eq. (1) reduces to

$$Q_{21} \cdot Q_{32} \cdot Q_{43} \cdot Q_{14} = I_3, \qquad (3)$$

where the transformation matrix $Q_{(i+1)i}$ is

$$\boldsymbol{Q}_{(i+1)i} = \begin{bmatrix} \cos\theta_i & -\cos\alpha_{(i+1)i}\sin\theta_i & \sin\alpha_{(i+1)i}\sin\theta_i \\ \sin\theta_i & \cos\alpha_{(i+1)i}\cos\theta_i & -\sin\alpha_{(i+1)i}\cos\theta_i \\ 0 & \sin\alpha_{(i+1)i} & \cos\alpha_{(i+1)i} \end{bmatrix}, \quad i=1,2,3,4, \quad (4)$$

which transforms the expression in the $(i+1)$ th coordinate system to the i th coordinate system, and when $i+1=5$, it is replaced by 1.
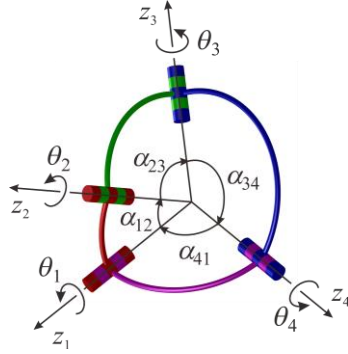

Fig. 3 A spherical 4R linkage

If a four-crease origami vertex is flat-foldable, its opposite sector angles should be supplementary [28]. Therefore, in its equivalent spherical 4R linkage (Fig. 3), following geometrical parameters can be defined in accordance with the D-H notation as shown in Fig. 2,

$$a_{12}=a_{23}=a_{34}=a_{41}=0, \quad \alpha_{12}=\pi-\alpha_{34}, \quad \alpha_{23}=\pi-\alpha_{41}, \quad R_1=R_2=R_3=R_4=0. \quad (5)$$

Substituting Eq. (5) to Eq. (3), the relationship between kinematic variables θ_i and θ_{i+1} ($i=1,2,3,4$) can be obtained,

$$\begin{aligned} &\cos\alpha_{(i+1)(i+2)}\cdot\sin\alpha_{i(i+1)}\cdot\sin\alpha_{(i-1)i}\cdot\cos\theta_i + \cos\alpha_{(i-1)i}\cdot\sin\alpha_{i(i+1)}\cdot\sin\alpha_{(i+1)(i+2)}\cdot\cos\theta_{i+1} \\ &+\cos\alpha_{i(i+1)}\cdot\sin\alpha_{(i+1)(i+2)}\cdot\sin\alpha_{(i-1)i}\cdot\cos\theta_i\cdot\cos\theta_{i+1} - \cos\alpha_{i(i+1)}\cdot\cos\alpha_{(i+1)(i+2)}\cdot\cos\alpha_{(i-1)i} \\ &-\sin\alpha_{(i+1)(i+2)}\cdot\sin\alpha_{(i-1)i}\cdot\sin\theta_i\cdot\sin\theta_{i+1} + \cos\alpha_{(i+2)(i+3)} = 0. \end{aligned} \quad (6)$$

Solving Eq. (6) by replacing $\sin\theta_i$, $\cos\theta_i$, $\sin\theta_{i+1}$ and $\cos\theta_{i+1}$ with the double angle

formula, we can obtain two solutions,

$$
\frac{\tan\dfrac{\theta_1}{2}}{\tan\dfrac{\theta_2}{2}} = -\frac{\sin\dfrac{\alpha_{23}-\alpha_{12}}{2}}{\sin\dfrac{\alpha_{23}+\alpha_{12}}{2}}, \quad \frac{\tan\dfrac{\theta_2}{2}}{\tan\dfrac{\theta_3}{2}} = \frac{\sin\dfrac{\alpha_{23}+\alpha_{12}}{2}}{\sin\dfrac{\alpha_{23}-\alpha_{12}}{2}},
$$
$$
\frac{\tan\dfrac{\theta_3}{2}}{\tan\dfrac{\theta_4}{2}} = \frac{\sin\dfrac{\alpha_{23}-\alpha_{12}}{2}}{\sin\dfrac{\alpha_{23}+\alpha_{12}}{2}}, \quad \frac{\tan\dfrac{\theta_4}{2}}{\tan\dfrac{\theta_1}{2}} = -\frac{\sin\dfrac{\alpha_{23}+\alpha_{12}}{2}}{\sin\dfrac{\alpha_{23}-\alpha_{12}}{2}},
$$

$$\tag{7a}$$

and

$$
\frac{\tan\dfrac{\theta_1}{2}}{\tan\dfrac{\theta_2}{2}} = -\frac{\cos\dfrac{\alpha_{23}-\alpha_{12}}{2}}{\cos\dfrac{\alpha_{23}+\alpha_{12}}{2}}, \quad \frac{\tan\dfrac{\theta_2}{2}}{\tan\dfrac{\theta_3}{2}} = -\frac{\cos\dfrac{\alpha_{23}+\alpha_{12}}{2}}{\cos\dfrac{\alpha_{23}-\alpha_{12}}{2}},
$$
$$
\frac{\tan\dfrac{\theta_3}{2}}{\tan\dfrac{\theta_4}{2}} = \frac{\cos\dfrac{\alpha_{23}-\alpha_{12}}{2}}{\cos\dfrac{\alpha_{23}+\alpha_{12}}{2}}, \quad \frac{\tan\dfrac{\theta_4}{2}}{\tan\dfrac{\theta_1}{2}} = \frac{\cos\dfrac{\alpha_{23}+\alpha_{12}}{2}}{\cos\dfrac{\alpha_{23}-\alpha_{12}}{2}}.
$$

$$\tag{7b}$$

It can be derived from Eq. (7a) that $\tan\dfrac{\theta_1}{2} = -\tan\dfrac{\theta_3}{2}$ while $\tan\dfrac{\theta_2}{2} = \tan\dfrac{\theta_4}{2}$, which means

θ_1 and θ_3 are of opposite signs whereas θ_2 and θ_4 are of the same. Eq. (7b) is on the

contrary with $\tan\dfrac{\theta_1}{2} = \tan\dfrac{\theta_3}{2}$ while $\tan\dfrac{\theta_2}{2} = -\tan\dfrac{\theta_4}{2}$. For a flat-foldable origami pattern,

the two creases around the minimum sector angle should be of opposite assignment as

a mountain or a valley crease, while the two creases around the maximum sector angle

are of the same assignment [28]. Assuming that α_{12} is the minimum angle, the two

solutions in Eq. (7a) and Eq. (7b) correspond to the two schemes of M-V assignment of

the four-crease origami vertex as shown in Fig. 4(a) and Fig. 4(b) respectively, where the

mountain creases are illustrated by solid lines, the valley creases by dashed lines, and φ_i is the dihedral angle of the facets with a common crease Z_i.
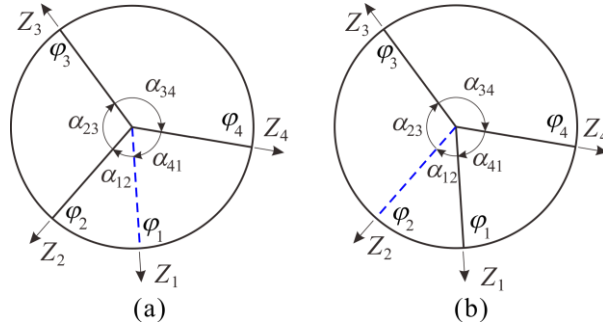
(a)　　　　　　　　(b)

Fig. 4   Four-crease origami vertices with two schemes of M-V assignment, (a) Vertex-I, and (b) Vertex-II.

The relationship between the kinematic variable θ_i and the dihedral angle φ_i is presented in Fig. 5, where we can find out that for a mountain crease, $\varphi_i = \pi - \theta_i$, and for a valley crease, $\varphi_i = \pi + \theta_i$. So the relationship is $\varphi_1 = \pi + \theta_1$, $\varphi_2 = \pi - \theta_2$, $\varphi_3 = \pi - \theta_3$, $\varphi_4 = \pi - \theta_4$ for Vertex-I, and $\varphi_1 = \pi - \theta_1$, $\varphi_2 = \pi + \theta_2$, $\varphi_3 = \pi - \theta_3$, $\varphi_4 = \pi - \theta_4$ for Vertex-II.

(a)　　　　　　　　(b)

Fig. 5   The relationship between the kinematic variable and the dihedral angle for (a) mountain crease, and (b) valley crease.

Thus in Vertex-I, we have,

$$\frac{\tan\dfrac{\varphi_1}{2}}{\tan\dfrac{\varphi_2}{2}}=\frac{\sin\dfrac{\alpha_{23}+\alpha_{12}}{2}}{\sin\dfrac{\alpha_{23}-\alpha_{12}}{2}}\;,\quad \frac{\tan\dfrac{\varphi_2}{2}}{\tan\dfrac{\varphi_3}{2}}=\frac{\sin\dfrac{\alpha_{23}-\alpha_{12}}{2}}{\sin\dfrac{\alpha_{23}+\alpha_{12}}{2}}\;,$$
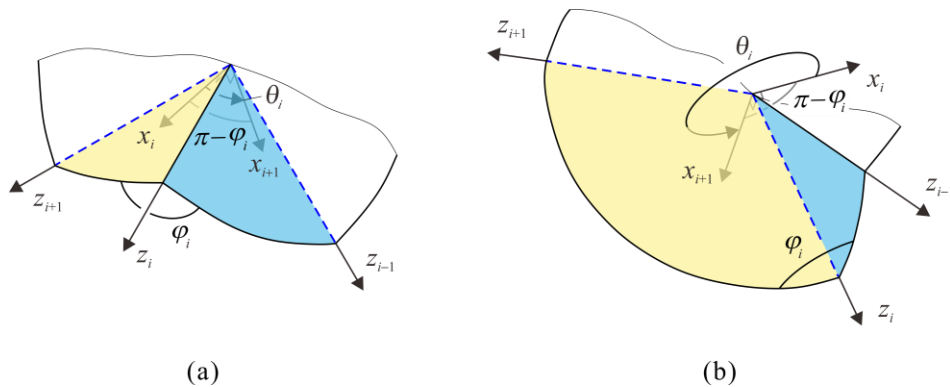
$$\frac{\tan\dfrac{\varphi_3}{2}}{\tan\dfrac{\varphi_4}{2}}=\frac{\sin\dfrac{\alpha_{23}+\alpha_{12}}{2}}{\sin\dfrac{\alpha_{23}-\alpha_{12}}{2}}\;,\quad \frac{\tan\dfrac{\varphi_4}{2}}{\tan\dfrac{\varphi_1}{2}}=\frac{\sin\dfrac{\alpha_{23}-\alpha_{12}}{2}}{\sin\dfrac{\alpha_{23}+\alpha_{12}}{2}}\;,$$

(8a)

and in Vertex-II,

$$\frac{\tan\dfrac{\varphi_1}{2}}{\tan\dfrac{\varphi_2}{2}}=\frac{\cos\dfrac{\alpha_{23}+\alpha_{12}}{2}}{\cos\dfrac{\alpha_{23}-\alpha_{12}}{2}}\;,\quad \frac{\tan\dfrac{\varphi_2}{2}}{\tan\dfrac{\varphi_3}{2}}=\frac{\cos\dfrac{\alpha_{23}-\alpha_{12}}{2}}{\cos\dfrac{\alpha_{23}+\alpha_{12}}{2}}\;,$$

$$\frac{\tan\dfrac{\varphi_3}{2}}{\tan\dfrac{\varphi_4}{2}}=\frac{\cos\dfrac{\alpha_{23}+\alpha_{12}}{2}}{\cos\dfrac{\alpha_{23}-\alpha_{12}}{2}}\;,\quad \frac{\tan\dfrac{\varphi_4}{2}}{\tan\dfrac{\varphi_1}{2}}=\frac{\cos\dfrac{\alpha_{23}-\alpha_{12}}{2}}{\cos\dfrac{\alpha_{23}+\alpha_{12}}{2}}\;.$$

(8b)

Figure 6(a) shows a generalized triangle twist origami pattern with a specific M-V assignment. Since a four-crease vertex in rigid origami is kinematically equivalent to a spherical $4R$ linkage, the triangle twist origami pattern can be modeled as a network of three spherical $4R$ linkages. Assuming $\alpha_{12}^{j}\ (j=a,b,c)$ be the minimum angle of the four-crease vertex, following geometrical parameters of the triangle twist origami pattern are set up,

$$\alpha_{41}^{a}=\pi-\alpha_{23}^{a}=\alpha\;,\;\; \alpha_{12}^{a}=\pi-\alpha_{34}^{a}=\gamma\;,\; 0<\gamma\leq\min\{\alpha,\pi-\alpha\}\;, \tag{9a}$$

$$\alpha_{41}^{b}=\pi-\alpha_{23}^{b}=\beta\;,\;\; \alpha_{12}^{b}=\pi-\alpha_{34}^{b}=\delta\;,\; 0<\delta\leq\min\{\beta,\pi-\beta\}\;, \tag{9b}$$

$$\alpha_{41}^{c}=\pi-\alpha_{23}^{c}=\pi-\alpha-\beta\;,\;\; \alpha_{12}^{c}=\pi-\alpha_{34}^{c}=\varepsilon\;,\; 0<\varepsilon\leq\min\{\alpha+\beta,\pi-\alpha-\beta\}\;, \tag{9c}$$

so the simplified representation of the triangle twist origami pattern is shown in Fig.

6(b).
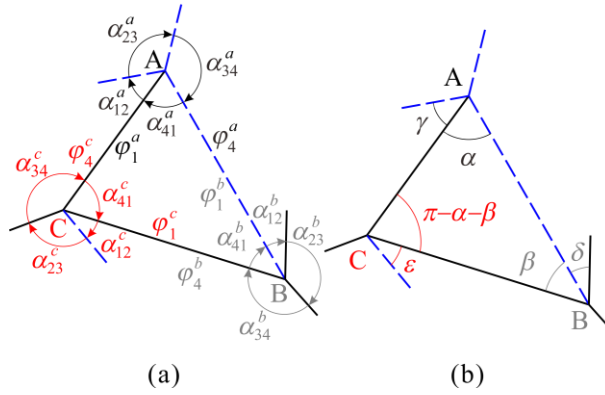
(a)　　　　　　　　(b)

Fig. 6　A generalized triangle twist origami pattern with a specific M-V assignment: (a)

the general representation, and (b) the simplified one.

In this case, vertices A and B are both Vertex-I, and vertex C is Vertex-II in Fig. 4.

The relationship of the dihedral angles φ_1^j and φ_4^j can be defined as

$\mu^j = \tan\dfrac{\varphi_4^j}{2} / \tan\dfrac{\varphi_1^j}{2}$ ($j = a, b, c$). Combining it with Eqs. (8) and (9), we have

$$\mu^a = \frac{\cos\dfrac{\alpha+\gamma}{2}}{\cos\dfrac{\alpha-\gamma}{2}}, \quad \mu^b = \frac{\cos\dfrac{\beta+\delta}{2}}{\cos\dfrac{\beta-\delta}{2}}, \quad \mu^c = \frac{\cos\dfrac{\alpha+\beta-\varepsilon}{2}}{\cos\dfrac{\alpha+\beta+\varepsilon}{2}}, \tag{10}$$

where $\cos\alpha \leq \mu^a < 1$, $\cos\beta \leq \mu^b < 1$, $1 < \mu^c \leq 1/\cos(\alpha+\beta)$, for $\alpha+\beta < \dfrac{\pi}{2}$, and

$\max\{0, \cos\alpha\} \leq \mu^a < 1$, $\max\{0, \cos\beta\} \leq \mu^b < 1$, $\mu^c > 1$, for $\alpha+\beta \geq \dfrac{\pi}{2}$.

Since each crease along the edge of the central triangle is shared by two adjacent

vertices as shown in Fig. 6(a), we have

$$\varphi_4^a = \varphi_1^b \ , \quad \varphi_4^b = \varphi_1^c \ , \quad \varphi_4^c = \varphi_1^a \ . \tag{11}$$

Further, the following relationship can be established,

$$\frac{\tan \dfrac{\varphi_4^a}{2}}{\tan \dfrac{\varphi_1^a}{2}} \cdot \frac{\tan \dfrac{\varphi_4^b}{2}}{\tan \dfrac{\varphi_1^b}{2}} \cdot \frac{\tan \dfrac{\varphi_4^c}{2}}{\tan \dfrac{\varphi_1^c}{2}} = 1 \ . \tag{12}$$

Therefore, the compatible condition of the triangle twist origami pattern [12] is

$$\mu^a \cdot \mu^b \cdot \mu^c = 1. \tag{13}$$

With defined values of α and β, assigning arbitrary values within the domain of definition in Eq. (9) to γ and δ, we can always find a ε to satisfy the compatible condition in Eq. (13) as

$$\varepsilon = 2\arctan \frac{\zeta - 1}{(\zeta + 1) \cdot \tan \dfrac{\alpha + \beta}{2}} \ , \quad \zeta = \frac{1}{\mu^a \cdot \mu^b} \ . \tag{14}$$

Once the value of ε obtained by Eq. (14) locates in the domain $(0, \pi)$, the triangle twist origami pattern is rigidly foldable.

Depending on the position relation of the three crease-pairs $Z_3^a \ \& \ Z_2^b$, $Z_3^b \ \& \ Z_2^c$ and $Z_3^c \ \& \ Z_2^a$, the triangle twist origami pattern can be divided into three types, where each crease-pair is intersected, or only one crease-pair is parallel, or each crease-pair is parallel as shown in Fig. 7(a)-(c) respectively.
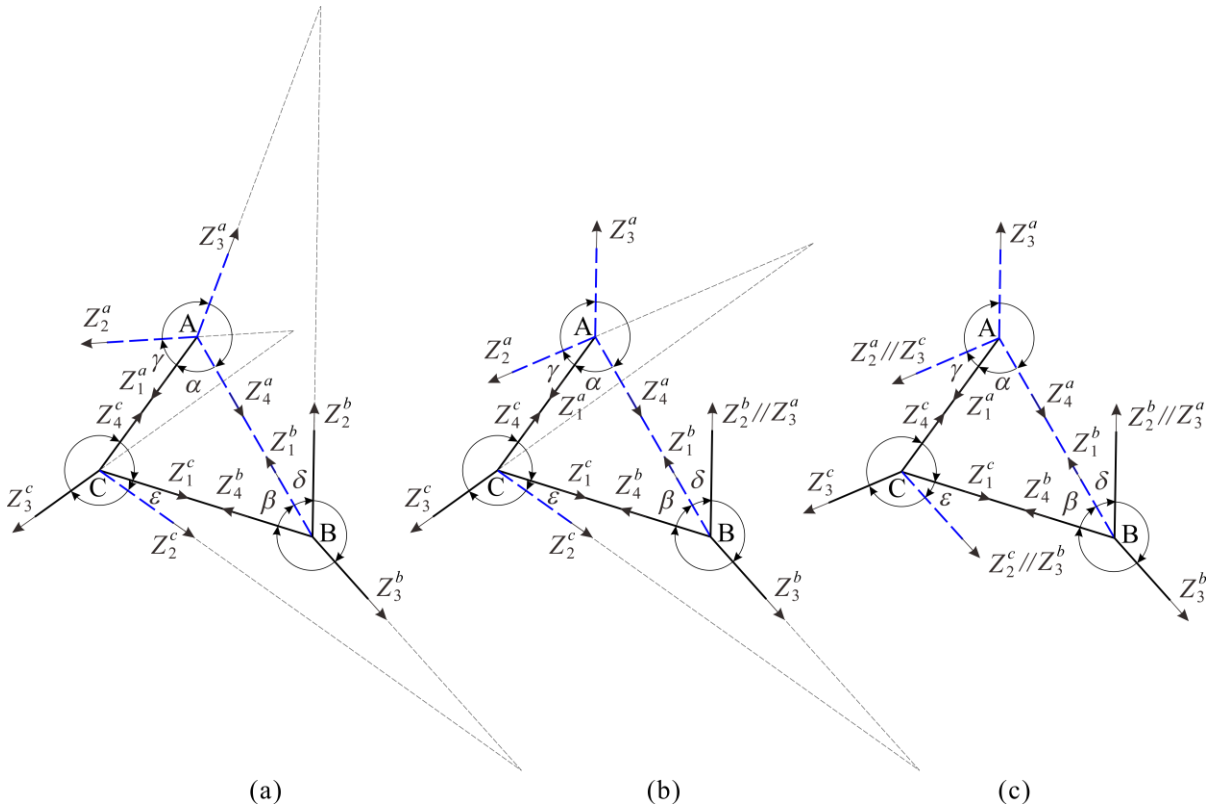
Fig. 7 Three types of the triangle twist origami patterns where (a) each crease-pair is intersected, or (b) only one crease-pair is parallel, or (c) each crease-pair is parallel.

When each crease-pair is intersected, we can always find a ε as Eq. (14) for any value of γ and δ in the domain of definition. This type of pattern is rigidly foldable once $\varepsilon \in (0, \pi)$.

When only one crease-pair is parallel, supposing that $Z_3^a // Z_2^b$, then $\gamma = \delta$, and ε can also be derived from Eq. (14). If $Z_3^b // Z_2^c$, then $\delta = \varepsilon$, and

$$\gamma = 2\arctan \frac{1-\zeta}{(\zeta+1)\cdot \tan\dfrac{\alpha}{2}}, \quad \zeta = \frac{1}{\mu^b \cdot \mu^c}. \tag{15}$$

If $Z_3^c // Z_2^a$, then $\varepsilon = \gamma$, and

$$\delta = 2\arctan\frac{1-\zeta}{(\zeta+1)\cdot\tan\dfrac{\beta}{2}}, \quad \zeta = \frac{1}{\mu^a \cdot \mu^c}.$$

(16)

Thus the pattern is also rigidly foldable with one parallel crease-pair when the calculated angle locates in the domain $(0, \pi)$.

When each crease-pair is parallel, then $\gamma = \delta = \varepsilon$, Eq. (13) can be rewritten as

$$\frac{\cos\dfrac{\alpha+\gamma}{2}}{\cos\dfrac{\alpha-\gamma}{2}} \cdot \frac{\cos\dfrac{\beta+\gamma}{2}}{\cos\dfrac{\beta-\gamma}{2}} \cdot \frac{\cos\dfrac{\alpha+\beta-\gamma}{2}}{\cos\dfrac{\alpha+\beta+\gamma}{2}} = 1,$$

(17)

which can be further simplified as

$$\sin\frac{\alpha}{2} \cdot \sin\frac{\beta}{2} = 0.$$

(18)

Since α and β are interior angles of a triangle, no solution of Eq. (18) exists. Therefore, the parallel triangle twist origami pattern is not rigidly foldable.

3. MOUNTAIN-VALLEY CREASE ASSIGNMENT OF THE TRIANGLE TWIST ORIGAMI PATTERN AND ITS EFFECT ON RIGID FOLDABILITY

We have analyzed the rigid foldability and motion of the triangle twist origami pattern with one specific scheme of M-V assignment in section 2. Since the rigid foldability of an origami pattern may vary with the change of M-V assignment, here we are going to find out all possible schemes of M-V assignment for the generalized triangle twist origami pattern and discuss their effect on rigid foldability.

According to the flat-foldable conditions of a four-crease vertex, the number difference between mountain creases and valley ones should be equal to two [28]. It

forms the criteria for determining schemes of M-V assignment, together with the condition on the opposite M-V assignment of the two creases around the minimum sector angle. Therefore, the M-V assignment of the generalized triangle twist origami pattern is related to the position of the minimum angle in the pattern. Considering the connection between adjacent vertices in a triangle twist origami pattern, α_{41} is always set as the interior angle of the central triangle. Since α_{12}, α_{23}, α_{34} and α_{41} could be chosen alternatively as the minimum angle, eight cases exist for one vertex in the triangle twist origami pattern. Combining repeated cases, the M-V assignment for one vertex in the triangle twist origami pattern can be classified into four types defined as Type P, Type Q, Type R and Type S in Fig. 8.
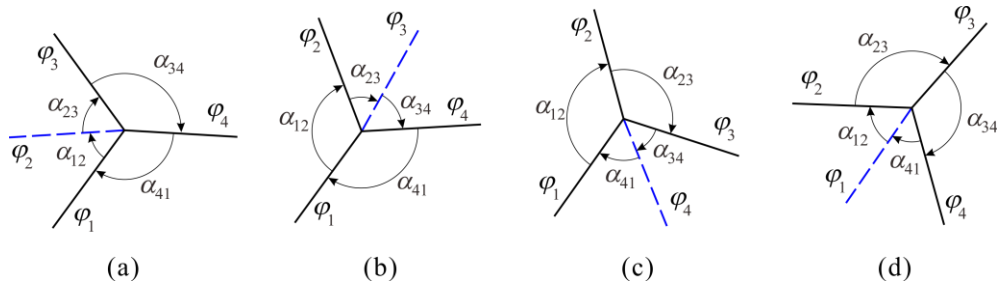
(a)   (b)   (c)   (d)

Fig. 8 Four types of M-V assignment of one vertex in the generalized triangle twist origami pattern where the minimum angle is (a) α_{12} or α_{23} for Type P, (b) α_{23} or α_{34} for Type Q, (c) α_{34} or α_{41} for Type R, and (d) α_{41} or α_{12} for Type S.

By defining $\mu_k = \tan\dfrac{\varphi_4}{2} / \tan\dfrac{\varphi_1}{2}$, where the subscript $k = p, q, r, s$ that represents the type of the vertex, kinematic relationship of the two dihedral angles φ_1 and φ_4

along the creases in the central triangle can be obtained. For Type P, it is a Vertex-II as shown in Fig. 4(b), and according to Eq. (8b), we have

$$\mu_p = \frac{\cos\dfrac{\alpha_{23}-\alpha_{12}}{2}}{\cos\dfrac{\alpha_{23}+\alpha_{12}}{2}} = \frac{\sin\dfrac{\alpha_{41}+\alpha_{12}}{2}}{\sin\dfrac{\alpha_{41}-\alpha_{12}}{2}} . \tag{19a}$$

For Type Q, it is a rotated Vertex-II as shown in Fig. 4(b), and according to Eq. (8b), we have

$$\mu_q = \frac{\cos\dfrac{\alpha_{34}+\alpha_{23}}{2}}{\cos\dfrac{\alpha_{34}-\alpha_{23}}{2}} = \frac{-\cos\dfrac{\alpha_{41}+\alpha_{12}}{2}}{\cos\dfrac{\alpha_{41}-\alpha_{12}}{2}} . \tag{19b}$$

For Type R, it is a rotated Vertex-I as shown in Fig. 4(a), and according to Eq. (8a), we have

$$\mu_r = \frac{\sin\dfrac{\alpha_{41}+\alpha_{12}}{2}}{\sin\dfrac{\alpha_{12}-\alpha_{41}}{2}} . \tag{19c}$$

And for Type S, it is Vertex-I as shown in Fig. 4(a), and according to Eq. (8a), we have

$$\mu_s = \frac{\sin\dfrac{\alpha_{23}-\alpha_{12}}{2}}{\sin\dfrac{\alpha_{23}+\alpha_{12}}{2}} = \frac{\cos\dfrac{\alpha_{41}+\alpha_{12}}{2}}{\cos\dfrac{\alpha_{41}-\alpha_{12}}{2}} . \tag{19d}$$

There are three vertices of a triangle twist origami pattern and each vertex has four types of M-V assignment, so $64\,(=4^3)$ combinations of vertices arrangements exist for the generalized triangle twist origami pattern. Considering that the crease common to adjacent vertices has the same assignment, only 32 schemes of M-V assignment are left as presented in Appendix A. Two special scenarios exist where the M-V assignment

would be duplicated. First, if we flip the paper, the mountain creases then become the valley creases. That is to say, these kinds of M-V assignment would be the inverted configurations. For example, the M-V assignment in Fig. 9(a) (PRR) is a duplicate of the one in Fig. A1 No.5 with the inverted configuration, where only the minimum angle of each vertex is presented and the character in the frame indicates the type of the vertex. Second, the M-V assignment would be duplicated if we change the vertex arrangement by rotating it along the center of the triangle in the triangle twist origami pattern. For example, the M-V assignment in Fig. 9(b) is a duplicate of the one in Fig. 9(a) obtained by rotation about the center of the triangle ABC. Considering the generality of the central triangle, the M-V assignment in Fig. 9(b) is equal to the one in Fig. 9(c) (RPR) that copied from Fig. A1 No.17. That is, the PRR twist in Fig. A1 No.5 and the RPR twist in Fig. A1 No.17 can be regarded as the same. As a result, twelve unique schemes of M-V assignment are obtained, which are denoted as PPP, PPQ, PQQ, PRR, PRS, PSS, QQQ, QRR, QRS, QSS, PSR and QSR as shown in Fig. 10, where the pattern as shown in Fig. 6 is a duplicate obtained by rotating the type of PSS twist as shown in Fig. 10(f).
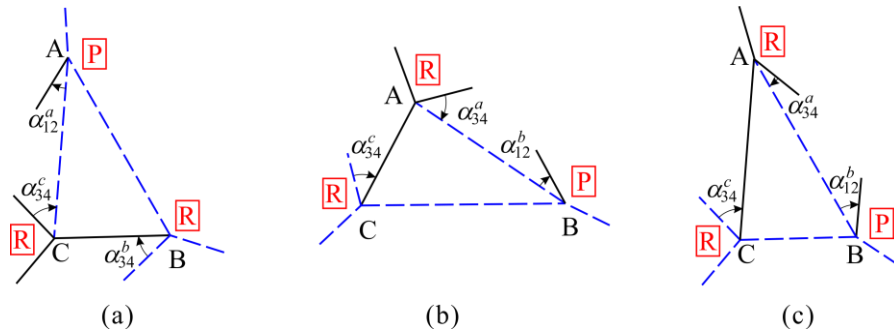
(a)　　　　　　　　　(b)　　　　　　　　　(c)

Fig. 9 Duplicated M-V assignments: (a) the M-V assignment obtained by flipping the paper in Fig. A1 No.5, (b) the one obtained by rotating (a) along the center of the triangle ABC, and (c) the one copied from Fig. A1 No.17.
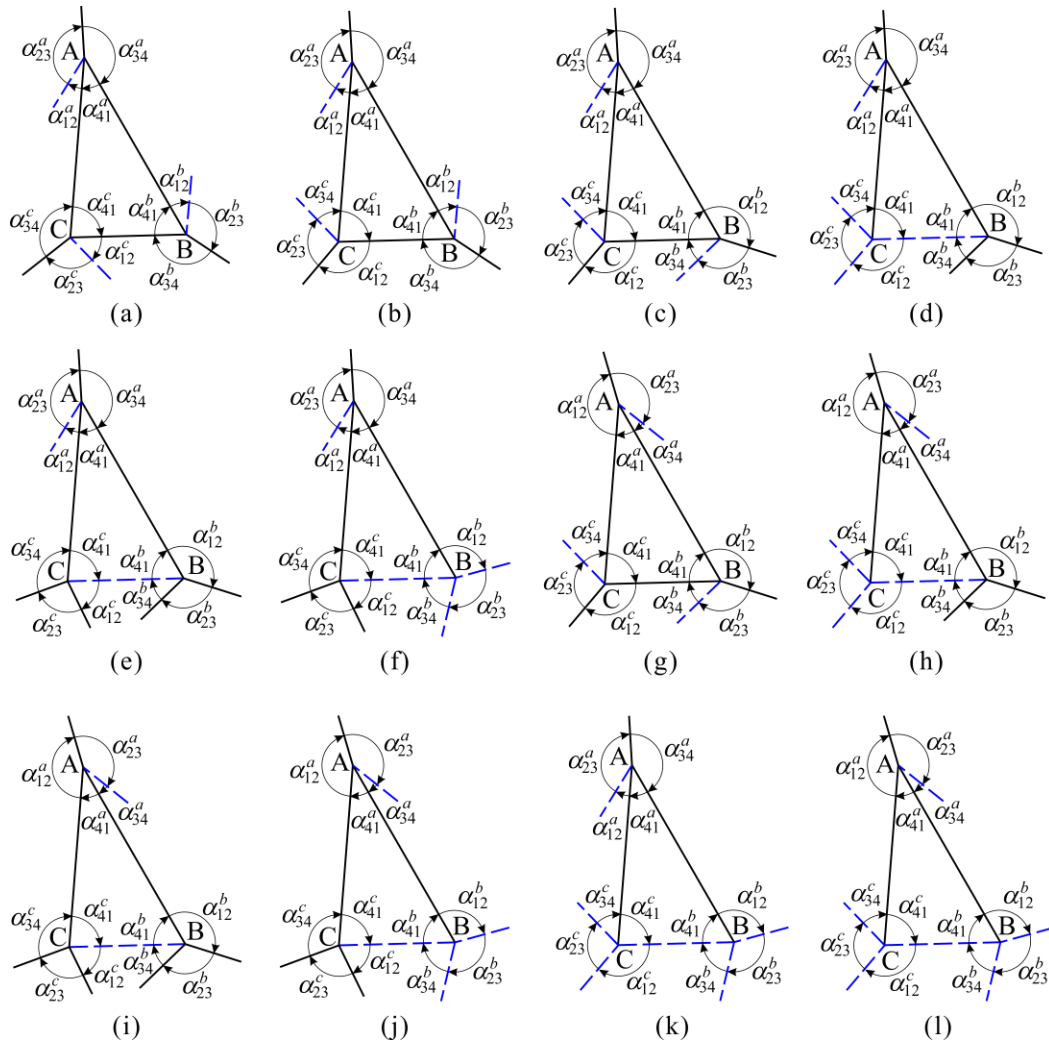
Fig. 10 Twelve unique schemes of M-V assignment of the generalized triangle twist

origami pattern with vertex-types being (a) PPP, (b) PPQ, (c) PQQ, (d) PRR, (e) PRS, (f)

PSS, (g)QQQ, (h) QRR, (i) QRS, (j) QSS, (k) PSR and (l) QSR.

From Fig. 10, we can see that there are two schemes of M-V assignment, PRS and

QRS (Fig. 10(e), (i)), each of which has seven mountain creases and two valley ones.

Another four schemes, PPP, PPQ, PQQ and QQQ (Fig. 10(a), (b), (c), (g)), have six

mountain creases and three valley ones respectively. Each one of the four schemes, PRR, PSS, QRR and QSS (Fig. 10(d), (f), (h), (j)), has five mountain creases and four valley ones. Two schemes, PSR and QSR (Fig. 10(k), (l)), exist with three mountain creases and six valley ones respectively. The difference between the schemes with identical numbers of mountain and valley creases is the position of the minimum angle, which affects the kinematics of each vertex and their compatibility. The detailed classification and rigidity of these schemes are represented as shown in Table A1 in Appendix A.

Similar to the analysis procedure in section 2, the relationships $\mu_i^j (i = 1, 2, ..., 12, \ j = a, b, c)$ between φ_1^j and φ_4^j are substituted to the compatible condition as Eq. (13) to find out the rigid foldability of all these types of triangle twist origami patterns with various M-V assignments. For the PPP twist (Fig. 10(a)), the μ_i^j of this type are

$$\mu_1^a = \frac{\sin\dfrac{\alpha+\gamma}{2}}{\sin\dfrac{\alpha-\gamma}{2}}, \quad \mu_1^b = \frac{\sin\dfrac{\beta+\delta}{2}}{\sin\dfrac{\beta-\delta}{2}}, \quad \mu_1^c = \frac{\cos\dfrac{\alpha+\beta-\varepsilon}{2}}{\cos\dfrac{\alpha+\beta+\varepsilon}{2}}, \tag{20}$$

with $\mu_1^a > 1$, $\mu_1^b > 1$, $\mu_1^c > 1$, so it is impossible to find solutions for Eq. (13). Therefore, the type of PPP twist is not rigidly foldable.

For the PPQ twist (Fig. 10(b)), the μ_i^j of this type are

$$\mu_2^a = \frac{\sin\dfrac{\alpha+\gamma}{2}}{\sin\dfrac{\alpha-\gamma}{2}}, \quad \mu_2^b = \frac{\sin\dfrac{\beta+\delta}{2}}{\sin\dfrac{\beta-\delta}{2}}, \quad \mu_2^c = \frac{-\sin\dfrac{\alpha+\beta-\varepsilon}{2}}{\sin\dfrac{\alpha+\beta+\varepsilon}{2}}, \tag{21}$$

with $\mu_2^a > 1$, $\mu_2^b > 1$, $\mu_2^c < 1$. When arbitrary values are assigned to α, β, γ and δ, we can find a ε according to the compatible condition in Eq. (13) as

$$\varepsilon = 2\arctan \frac{(\zeta_2 + 1) \cdot \tan \dfrac{\alpha + \beta}{2}}{1 - \zeta_2}, \quad \zeta_2 = \frac{1}{\mu_2^a \cdot \mu_2^b}. \tag{22}$$

Therefore, the type of PPQ twist is rigidly foldable once the obtained ε is within the range $(0, \pi)$.

All rigid foldability of the triangle twist origami patterns with other schemes of M-V assignment are analyzed in a similar way, which are presented in the Appendix B. In summary, only the PPQ, PQQ, PRS, PSS, QRR, QRS, PSR and QSR twists as shown in Fig. 10(b), (c), (e), (f), (h), (i), (k) and (l) are rigidly foldable, whereas the PPP, PRR, QQQ and QSS twists not. It should be noted that for a given M-V assignment of the triangle twist origami pattern within these eight types, the rigid foldability depends on the choice of design parameters as well. For example, the triangle twist origami pattern with $\alpha = 30^{\circ}$, $\beta = 80^{\circ}$, $\gamma = 90^{\circ}$, $\delta = 45^{\circ}$ and a calculated $\varepsilon = 7.04^{\circ}$ is rigidly foldable. However, when we change it to $\alpha = \beta = 60^{\circ}$ while $\gamma = 90^{\circ}$ and $\delta = 45^{\circ}$ unchanged, it is impossible to find a compatible ε for the pattern. That is, the triangle twist origami pattern becomes a non-rigid case. Therefore, we can design rigid or non-rigid triangle twist origami patterns by choosing proper M-V assignments and geometrical parameters according to our demands.

4. DERIVED 6*R* LINKAGES FROM THE GENERALIZED TRIANGLE TWIST PATTERN

Although the M-V assignment has an impact on rigid foldability of the generalized triangle twist origami pattern, it does not affect geometric conditions of its kinematically equivalent spherical linkages. Here we use the generalized triangle twist presented in section 2 to demonstrate the derivation of spatial 6*R* linkage from this pattern. Considering geometric conditions in Eq. (9), there are five design parameters α, β, γ, δ and ε for this pattern, whereas only four are independent. A physical origami model of the triangle twist origami pattern and its corresponding folding process are designed as shown in Fig. 11(a). Since the vertices A, B and C always keep in a single plane, so the central triangle ABC can be removed without affecting the motion of the pattern. Then a triangle twist kirigami pattern, which has only six creases as shown in Fig. 11(b), is obtained.

Recalling the relationship between mechanisms and origami patterns, a network of three spherical 4*R* linkages that corresponds to the triangle twist origami pattern in Fig. 11(a), can be built as shown in Fig. 12(a). Creases of vertices A, B and C are equivalent to joints a_i, b_i and c_i respectively, where joints a_4 & b_1, b_4 & c_1 and c_4 & a_1 are coaxial. The adjacent links a_3a_4 in the spherical 4*R* linkage **A** and b_1b_2 in the spherical 4*R* linkage **B** are connected into one rigid body, and the same connection method is applied to other adjacent links in Fig. 12(a), such as links a_4a_1 & b_4b_1, b_3b_4 & c_1c_2, b_4b_1 & c_4c_1, c_3c_4 & a_1a_2 and c_4c_1 & a_4a_1. When the origami pattern is rigid with one degree of freedom (DOF), its corresponding linkage network is also one DOF.

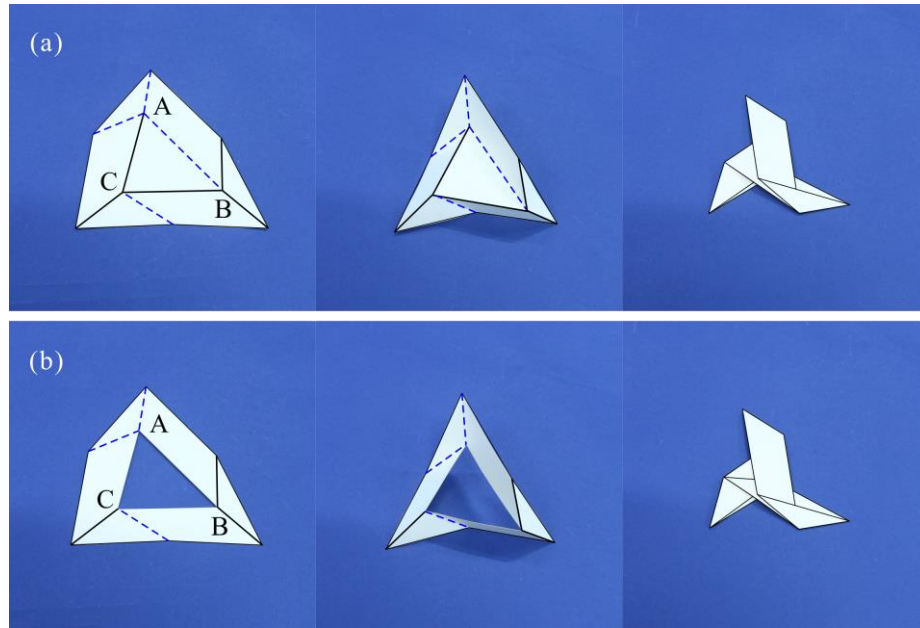Fig. 11 Physical triangle twist models with $\alpha = 55°$, $\beta = 50°$, $\gamma = 50°$, $\delta = 45°$ and $\varepsilon = 35.44°$ for (a) origami pattern, and (b) kirigami pattern.
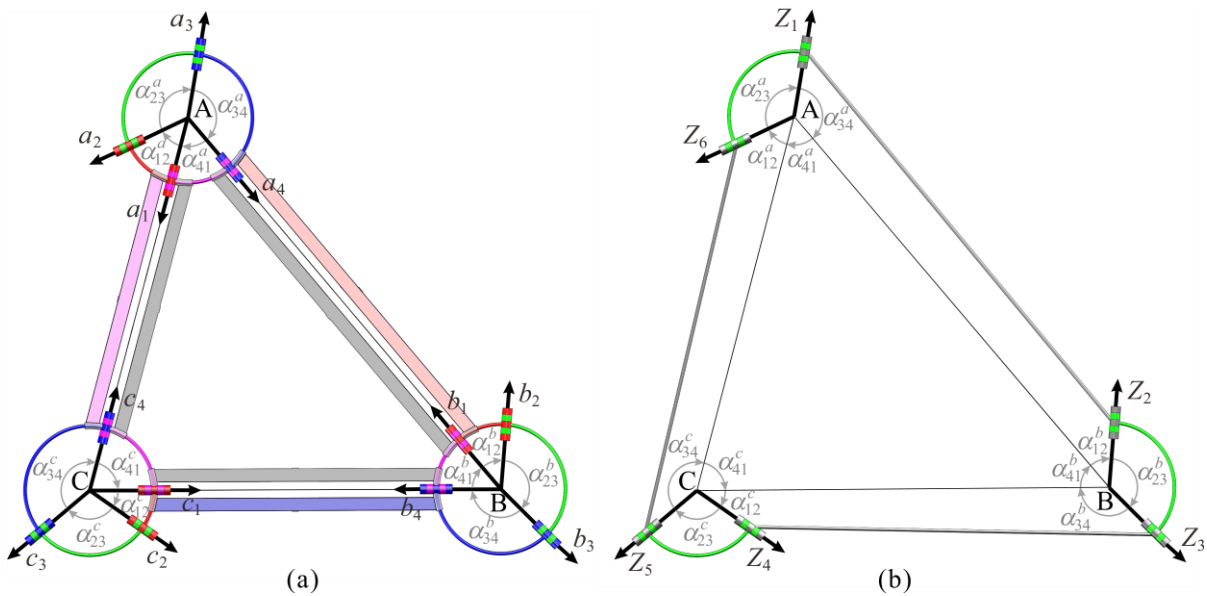

Fig. 12 Equivalent mechanisms of the generalized triangle twist: (a) the network of three spherical 4R linkages for the origami pattern, and (b) the derived overconstrained 6R linkage for the kirigami pattern.

Once the central triangle is removed, a mobile linkage from the kirigami pattern in Fig. 11(b), can also be built as a 6R linkage, see Fig. 12(b), after joints in the central triangle being removed, and joints a_3 & b_2 being connected by one link, so do joints b_3 & c_2 and c_3 & a_2. So the derived 6R linkage in Fig. 12(b) should also have one DOF as the network of spherical 4R linkages in Fig. 12(a). The six joints in the new derived 6R linkage have identical motion as joints a_3, b_2, b_3, c_2, c_3 and a_2 in the network of three spherical 4R linkages. Therefore, the kinematic analysis in section 2 can be applicable to the new 6R linkage as well.

It has been proved that the generalized triangle twist origami pattern in section 2 is rigidly foldable except for the parallel twist. The derived 6R linkages from kirigami patterns of the two rigidly foldable triangle twists will be discussed next. First considering the case where each crease-pair is intersected, the links have zero lengths with $\gamma \neq \delta$ correspondingly. The D-H notations of this new 6R linkage are depicted in Fig. 13(a). The axes of adjacent rotation joints intersect, and the intersection points of Z_6 & Z_1, Z_2 & Z_3, Z_4 & Z_5, Z_1 & Z_2, Z_3 & Z_4 and Z_5 & Z_6 are denoted as A, B, C, D, E and F respectively. Suppose the length of edge AB in the central triangle be L. The geometrical parameters of the 6R linkage can be calculated as follows.

$$a_{12} = a_{23} = a_{34} = a_{45} = a_{56} = a_{61} = 0, \tag{23a}$$

$$\begin{aligned}
&\alpha_{12} = 2\pi - \gamma + \delta, \alpha_{23} = \pi - \beta, \alpha_{34} = 2\pi - \delta + \varepsilon, \\
&\alpha_{45} = \alpha + \beta, \alpha_{56} = \gamma - \varepsilon, \alpha_{61} = \pi - \alpha,
\end{aligned} \tag{23b}$$

$$R_1 = \overline{AD} = \left|\frac{\sin \delta}{\sin(\gamma - \delta)}\right| \cdot L,$$

$$R_2 = -\overline{BD} = -\left|\frac{\sin \gamma}{\sin(\gamma - \delta)}\right| \cdot L,$$

$$R_3 = \overline{BE} = \left|\frac{\sin \varepsilon}{\sin(\delta - \varepsilon)}\right| \cdot \frac{L \sin \alpha}{\sin(\alpha + \beta)},$$

$$R_4 = -\overline{CE} = -\left|\frac{\sin \delta}{\sin(\delta - \varepsilon)}\right| \cdot \frac{L \sin \alpha}{\sin(\alpha + \beta)},$$ (23c)

$$R_5 = -\overline{CF} = -\left|\frac{\sin \gamma}{\sin(\gamma - \varepsilon)}\right| \cdot \frac{L \sin \beta}{\sin(\alpha + \beta)},$$

$$R_6 = \overline{AF} = \left|\frac{\sin \varepsilon}{\sin(\gamma - \varepsilon)}\right| \cdot \frac{L \sin \beta}{\sin(\alpha + \beta)},$$

where γ, δ and ε should satisfy Eqs. (9) and (14). According to Eq. (23c), the relationship $R_1 \cdot R_3 \cdot R_5 + R_2 \cdot R_4 \cdot R_6 = 0$ holds and all lengths of the links are zero in Eq. (23a), which reveals that the derived 6R linkage is actually a variation of doubly collapsible octahedral Bricard [29]. The kinematic relationship of the derived 6R linkage is

$$\tan\frac{\theta_2}{2} = \frac{\cos\dfrac{\alpha - \gamma}{2}\cos\dfrac{\beta - \delta}{2}}{\cos\dfrac{\alpha + \gamma}{2}\cos\dfrac{\beta + \delta}{2}} \cdot \tan\frac{\theta_1}{2}, \quad \tan\frac{\theta_3}{2} = \frac{\cos\dfrac{\alpha - \gamma}{2}}{\cos\dfrac{\alpha + \gamma}{2}} \cdot \tan\frac{\theta_1}{2},$$ (24)

$$\theta_4 = -\theta_1, \quad \theta_5 = \theta_2, \quad \theta_6 = \theta_3.$$

It can be seen that the kinematics of the derived doubly collapsible octahedral Bricard is not related to the value of L. It is determined by the relative position of their axes. Kinematic paths of an instance with $\alpha = 55°$, $\beta = 50°$, $\gamma = 50°$, $\delta = 45°$ and $\varepsilon = 35.44°$ are plotted as solid lines in Fig. 14.
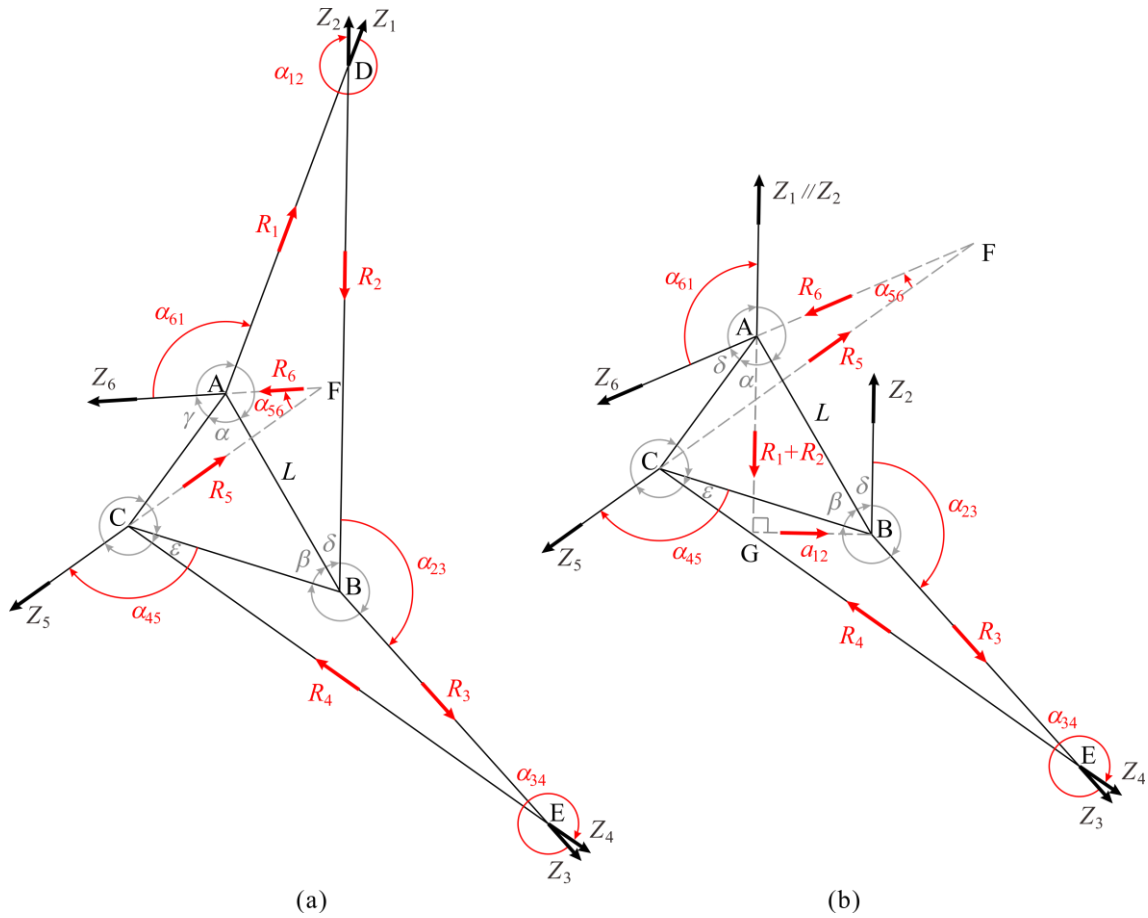
Fig. 13 Schematic diagrams of the derived overconstrained 6*R* linkages when (a) $\gamma \neq \delta$, and (b) $\gamma = \delta$.

Fig. 14 Kinematic paths of the derived overconstrained 6*R* linkages when each crease-pair is intersected with $\alpha = 55°$, $\beta = 50°$, $\gamma = 50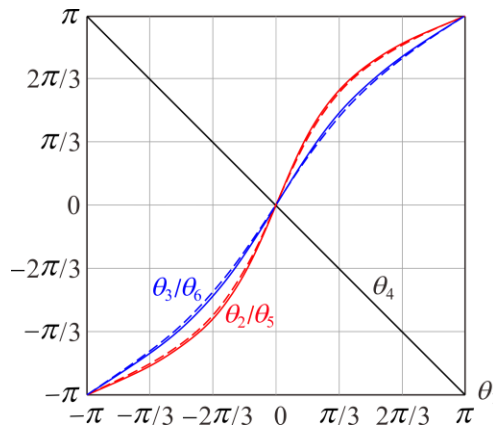°$, $\delta = 45°$, $\varepsilon = 35.44°$ as solid lines and when only one crease-pair is parallel with $\alpha = 55°$, $\beta = 50°$, $\gamma = \delta = 45°$, $\varepsilon = 33.52°$ as dashed lines.

Then consider the second case in which only one crease-pair is parallel, that is, the length of one link is non-zero by setting $\gamma = \delta$, see Fig. 13(b). In this case, the axis Z_1 is parallel to Z_2, and GB is their common perpendicular. Z_6 & Z_1, Z_2 & Z_3, Z_4 & Z_5, Z_3 & Z_4 and Z_5 & Z_6 intersect at the points A, B, C, E and F respectively. The length of link 12 is the distance between the parallel crease-pair, whereas those of all the other links and the twist angle of link 12 are zero. The geometrical parameters of the 6*R* linkage are

$$a_{12} = \overline{GB} = L \cdot \sin \delta ,$$
$$a_{23} = a_{34} = a_{45} = a_{56} = a_{61} = 0 ,$$

(25a)

$$\alpha_{12} = 0 , \quad \alpha_{23} = \pi - \beta , \quad \alpha_{34} = 2\pi - \delta + \varepsilon ,$$
$$\alpha_{45} = \alpha + \beta , \quad \alpha_{56} = \delta - \varepsilon , \quad \alpha_{61} = \pi - \alpha ,$$

(25b)

$$R_1 + R_2 = -L \cdot \cos \delta ,$$
$$R_3 = \overline{BE} = \left| \frac{\sin \varepsilon}{\sin(\delta - \varepsilon)} \right| \cdot \frac{L \sin \alpha}{\sin(\alpha + \beta)} ,$$
$$R_4 = -\overline{CE} = -\left| \frac{\sin \delta}{\sin(\delta - \varepsilon)} \right| \cdot \frac{L \sin \alpha}{\sin(\alpha + \beta)} ,$$
$$R_5 = -\overline{CF} = -\left| \frac{\sin \delta}{\sin(\delta - \varepsilon)} \right| \cdot \frac{L \sin \beta}{\sin(\alpha + \beta)} ,$$
$$R_6 = \overline{AF} = \left| \frac{\sin \varepsilon}{\sin(\delta - \varepsilon)} \right| \cdot \frac{L \sin \beta}{\sin(\alpha + \beta)} .$$

(25c)

It is found that $R_1 \cdot R_3 \cdot R_5 + R_2 \cdot R_4 \cdot R_6 = \dfrac{L^3 \cdot \sin \alpha \cdot \sin \beta \cdot \sin \delta \cdot \cos \delta \cdot \sin \varepsilon}{\sin^2(\alpha + \beta) \cdot \sin^2(\delta - \varepsilon)}$ from Eq. (25c) for the 6*R* linkage derived from the triangle twist kirigami pattern with only one parallel crease-pair. It neither satisfies the geometric conditions of doubly collapsible octahedral Bricard nor other existed overconstrained 6*R* linkages, such as Bricard linkages [30] and Bennett-based overconstrained linkages [31] etc., which indicates a

new type of overconstrained 6*R* linkage is obtained. Similarly, the kinematic relationship of this linkage is obtained by making $\gamma = \delta$ in Eq. (24). Changing geometrical parameters of the exemplified derived 6*R* linkage to $\gamma = 45°$, $\varepsilon = 33.52°$ while keeping other parameters identical to the previous case, the kinematic paths are plotted as dashed lines in Fig. 14. It can be found that both the geometrical parameters and kinematic paths differ little, which indicates that the new derived overconstrained 6*R* linkage could be treated as an extension of the doubly collapsible octahedral Bricard.

5. CONCLUSIONS

This paper has presented the rigid foldability and motion of the generalized triangle twist origami pattern with varying geometrical parameters and M-V assignments. They have been analyzed based on the kinematic equivalence between the rigid origami pattern and the network of spherical linkages. Twelve unique schemes of M-V assignment of the generalized triangle twist origami pattern have been found. However, only eight types are possible to be rigidly foldable. The compatible conditions have been derived for these types of triangle twist origami patterns. Furthermore, the rigid foldability has been discussed according to the position relation of three crease-pairs around edges of the central triangle in the triangle twist origami pattern. It has been found that the triangle twist origami pattern is rigidly foldable when at least one crease-pair is not parallel.

In addition, a triangle twist kirigami pattern has been developed by removing the central triangle in the rigid origami pattern. A variation of doubly collapsible octahedral

Bricard has been derived from the triangle twist kirigami pattern where each crease-pair is intersected. And a new type of overconstrained 6R linkage has been obtained when only one crease-pair is parallel.

To conclude, the thorough study on rigid foldability and motion of the generalized triangle twist pattern lays the theoretical foundation for its application as a modular unit of tessellation or a feasible design for origami robots. The proposed approach of generating new linkages from the triangle twist kirigami pattern opens up a new way to construct single-loop overconstrained linkages from the network of spherical linkages. It can be readily extended to other types of origami patterns.

APPENDIX

A. SCHEMES OF M-V ASSIGNMENT OF THE GENERALIZED TRIANGLE TWIST

    ORIGAMI PATTERN

Considering that the crease common to adjacent vertices has the same assignment, there are 32 schemes of M-V assignment for the generalized triangle twist origami pattern as given in Fig. A1, where only the minimum angle of each vertex is presented and the character in the frame indicates the type of the vertex.

Eliminating the duplicated cases, twelve unique schemes of M-V assignment are obtained, which are denoted as PPP, PPQ, PQQ, PRR, PRS, PSS, QQQ, QRR, QRS, QSS, PSR and QSR. The classification and rigidity of these schemes are listed in Table A1.

Fig. A1 All possible schemes of M-V assignment of the generalized triangle twist origami pattern: No.1 PPP, No.2 PPQ, No.3 PQP, No.4 PQQ, No.5 PRR, No.6 PRS, No.7 PSR, No.8 PSS, No.9 QPP, No.10 QPQ, No.11 QQP, No.12 QQQ, No.13 QRR, No.14 QRS, No.15 QSR, No.16 QSS, No.17 RPR, No.18 RPS, No.19 RQR, No.20 RQS, No.21 RRP, No.22 RRQ, No.23 RSP, No.24 RSQ, No.25 SPR, No.26 SPS, No.27 SQR, No.28 SQS, No.29 SRP, No.30 SRQ, No.31 SSP, and No.32 SSQ.
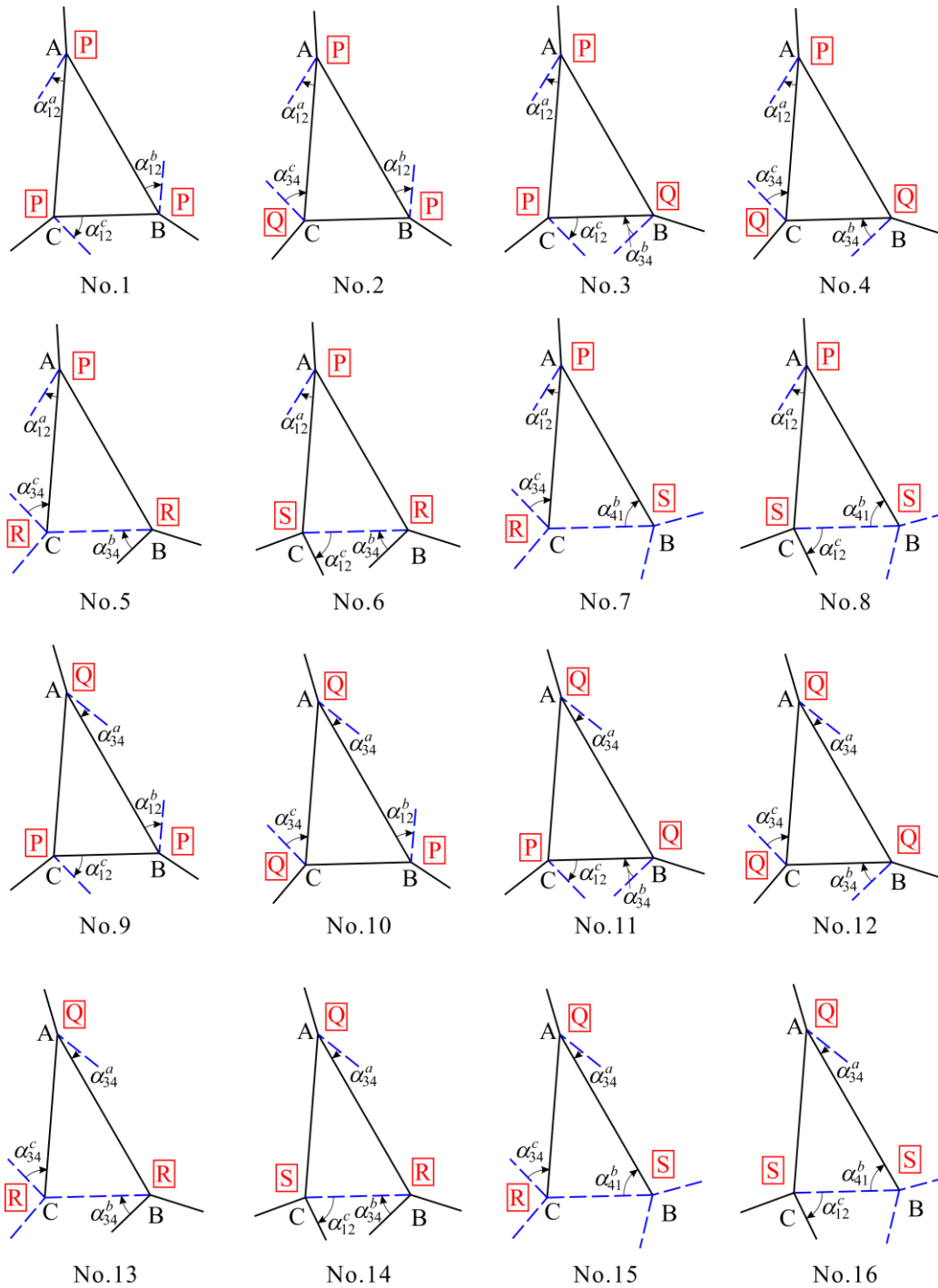
Fig. A1 All possible schemes of M-V assignment of the generalized triangle twist origami pattern: No.1 PPP, No.2 PPQ, No.3 PQP, No.4 PQQ, No.5 PRR, No.6 PRS, No.7 PSR, No.8 PSS, No.9 QPP, No.10 QPQ, No.11 QQP, No.12 QQQ, No.13 QRR, No.14 QRS, No.15 QSR, No.16 QSS, No.17 RPR, No.18 RPS, No.19 RQR, No.20 RQS, No.21 RRP, No.22 RRQ, No.23 RSP, No.24 RSQ, No.25 SPR, No.26 SPS, No.27 SQR, No.28 SQS, No.29 SRP, No.30 SRQ, No.31 SSP, and No.32 SSQ. (Continued)
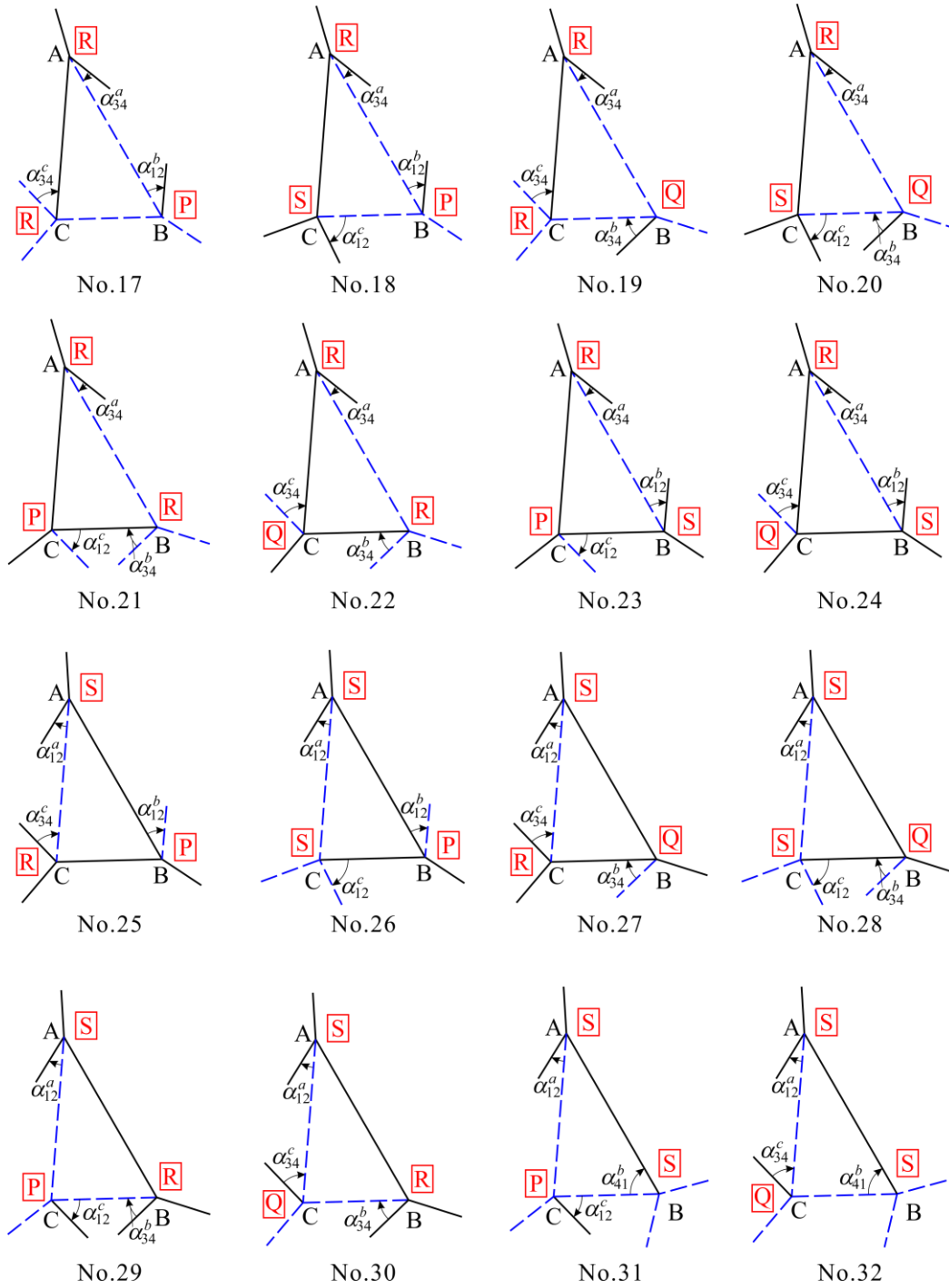
Table A1 Classification of M-V assignments for the generalized triangle twist origami

pattern

Number of mountain creases	Number of valley creases	Schemes of M-V assignment	Duplicated schemes of M-V assignment	Rigidity
7	2	PRS (Fig. A1 No.6)	RSP (Fig. A1 No.23), SPR (Fig. A1 No.25)	Rigid
		QRS (Fig. A1 No.14)	RSQ (Fig. A1 No.24), SQR (Fig. A1 No.27)	Rigid
6	3	PPP (Fig. A1 No.1)	non-existent	Non-rigid
		PPQ (Fig. A1 No.2)	PQP (Fig. A1 No.3), QPP(Fig. A1 No.9)	Rigid
		PQQ (Fig. A1 No.4)	QPQ (Fig. A1 No.10), QQP (Fig. A1 No.11)	Rigid
		QQQ (Fig. A1 No.12)	non-existent	Non-rigid
5	4	PRR (Fig. A1 No.5)	RPR (Fig. A1 No.17), RRP (Fig. A1 No.21)	Non-rigid
		PSS (Fig. A1 No.8)	SPS (Fig. A1 No.26), SSP (Fig. A1 No.31)	Rigid
		QRR (Fig. A1 No.13)	RQR (Fig. A1 No.19), RRQ (Fig. A1 No.22)	Rigid
		QSS (Fig. A1 No.16)	SQS (Fig. A1 No.28), SSQ (Fig. A1 No.32)	Non-rigid
3	6	PSR (Fig. A1 No.7)	RPS (Fig. A1 No.18), SRP (Fig. A1 No.29)	Rigid
		QSR (Fig. A1 No.15)	RQS (Fig. A1 No.20), SRQ (Fig. A1 No.30)	Rigid

B. RIGID FOLDABILITY OF TRIANGLE TWIST ORIGAMI PATTERNS WITH VARIOUS

M-V ASSIGNMENTS

For the PQQ twist (Fig. 10(c)), the μ_i^j of this type are

$$\mu_3^a = \frac{\sin\dfrac{\alpha+\gamma}{2}}{\sin\dfrac{\alpha-\gamma}{2}}, \quad \mu_3^b = \frac{-\cos\dfrac{\beta+\delta}{2}}{\cos\dfrac{\beta-\delta}{2}}, \quad \mu_3^c = \frac{-\sin\dfrac{\alpha+\beta-\varepsilon}{2}}{\sin\dfrac{\alpha+\beta+\varepsilon}{2}}, \tag{B1}$$

with $\mu_3^a > 1$, $\mu_3^b < 1$, $\mu_3^c < 1$. When arbitrary values are assigned to α, β, γ and δ, we can find a ε according to the compatible condition in Eq. (13) as

$$\varepsilon = 2\arctan\frac{(\zeta_3+1)\cdot\tan\dfrac{\alpha+\beta}{2}}{1-\zeta_3}, \quad \zeta_3 = \frac{1}{\mu_3^a\cdot\mu_3^b}. \tag{B2}$$

Therefore, the type of PQQ twist is rigidly foldable once the obtained ε is within the range $(0, \pi)$.

For the PRR twist (Fig. 10(d)), the μ_i^j of this type are

$$\mu_4^a = \frac{\sin\dfrac{\alpha+\gamma}{2}}{\sin\dfrac{\alpha-\gamma}{2}}, \quad \mu_4^b = \frac{\sin\dfrac{\beta+\delta}{2}}{\sin\dfrac{\delta-\beta}{2}}, \quad \mu_4^c = \frac{-\cos\dfrac{\alpha+\beta-\varepsilon}{2}}{\cos\dfrac{\alpha+\beta+\varepsilon}{2}}, \tag{B3}$$

with $\mu_4^a > 1$, $\mu_4^b > 1$, $\mu_4^c > 1$, so it is impossible to find solutions for Eq. (13). Therefore, the type of PRR twist is not rigidly foldable.

For the PRS twist (Fig. 10(e)), the μ_i^j of this type are

$$\mu_5^a = \frac{\sin\dfrac{\alpha+\gamma}{2}}{\sin\dfrac{\alpha-\gamma}{2}}, \quad \mu_5^b = \frac{\sin\dfrac{\beta+\delta}{2}}{\sin\dfrac{\delta-\beta}{2}}, \quad \mu_5^c = \frac{\sin\dfrac{\alpha+\beta-\varepsilon}{2}}{\sin\dfrac{\alpha+\beta+\varepsilon}{2}}, \tag{B4}$$

with $\mu_5^a > 1$, $\mu_5^b > 1$, $\mu_5^c < 1$. When arbitrary values are assigned to α, β, γ and δ, we can find a ε according to the compatible condition in Eq. (13) as

$$\varepsilon = 2\arctan\frac{(1-\zeta_5)\cdot\tan\dfrac{\alpha+\beta}{2}}{\zeta_5+1}, \quad \zeta_5 = \frac{1}{\mu_5^a\cdot\mu_5^b}. \tag{B5}$$

Therefore, the type of PRS twist is rigidly foldable once the obtained ε is within the range $(0,\pi)$.

For the PSS twist (Fig. 10(f)), the μ_i^j of this type are

$$\mu_6^a = \frac{\sin\dfrac{\alpha+\gamma}{2}}{\sin\dfrac{\alpha-\gamma}{2}}, \quad \mu_6^b = \frac{\cos\dfrac{\beta+\delta}{2}}{\cos\dfrac{\beta-\delta}{2}}, \quad \mu_6^c = \frac{\sin\dfrac{\alpha+\beta-\varepsilon}{2}}{\sin\dfrac{\alpha+\beta+\varepsilon}{2}}, \tag{B6}$$

with $\mu_6^a > 1$, $\mu_6^b < 1$, $\mu_6^c < 1$. When arbitrary values are assigned to α, β, γ and δ, we can find a ε according to the compatible condition in Eq. (13) as

$$\varepsilon = 2\arctan\frac{(1-\zeta_6)\cdot\tan\dfrac{\alpha+\beta}{2}}{\zeta_6+1}, \quad \zeta_6 = \frac{1}{\mu_6^a\cdot\mu_6^b}. \tag{B7}$$

Therefore, the type of PSS twist is rigidly foldable once the obtained ε is within the range $(0,\pi)$.

For the QQQ twist (Fig. 10(g)), the μ_i^j of this type are

$$\mu_7^a = \frac{-\cos\dfrac{\alpha+\gamma}{2}}{\cos\dfrac{\alpha-\gamma}{2}}, \quad \mu_7^b = \frac{-\cos\dfrac{\beta+\delta}{2}}{\cos\dfrac{\beta-\delta}{2}}, \quad \mu_7^c = \frac{-\sin\dfrac{\alpha+\beta-\varepsilon}{2}}{\sin\dfrac{\alpha+\beta+\varepsilon}{2}}, \tag{B8}$$

with $\mu_7^a < 1$, $\mu_7^b < 1$, $\mu_7^c < 1$, so it is impossible to find solutions for Eq. (13). Therefore, the type of QQQ twist is not rigidly foldable.

For the QRR twist (Fig. 10(h)), the μ_i^j of this type are

$$\mu_8^a = \frac{-\cos\dfrac{\alpha+\gamma}{2}}{\cos\dfrac{\alpha-\gamma}{2}}\,,\quad \mu_8^b = \frac{\sin\dfrac{\beta+\delta}{2}}{\sin\dfrac{\delta-\beta}{2}}\,,\quad \mu_8^c = \frac{-\cos\dfrac{\alpha+\beta-\varepsilon}{2}}{\cos\dfrac{\alpha+\beta+\varepsilon}{2}}\,, \tag{B9}$$

with $\mu_8^a < 1$, $\mu_8^b > 1$, $\mu_8^c > 1$. When arbitrary values are assigned to α, β, γ and δ, we can find a ε according to the compatible condition in Eq. (13) as

$$\varepsilon = 2\arctan\frac{\zeta_8+1}{(\zeta_8-1)\cdot\tan\dfrac{\alpha+\beta}{2}}\,,\quad \zeta_8 = \frac{1}{\mu_8^a\cdot\mu_8^b}\,. \tag{B10}$$

Therefore, the type of QRR twist is rigidly foldable once the obtained ε is within the range $(0,\pi)$.

For the QRS twist (Fig. 10(i)), the μ_i^j of this type are

$$\mu_9^a = \frac{-\cos\dfrac{\alpha+\gamma}{2}}{\cos\dfrac{\alpha-\gamma}{2}}\,,\quad \mu_9^b = \frac{\sin\dfrac{\beta+\delta}{2}}{\sin\dfrac{\delta-\beta}{2}}\,,\quad \mu_9^c = \frac{\sin\dfrac{\alpha+\beta-\varepsilon}{2}}{\sin\dfrac{\alpha+\beta+\varepsilon}{2}}\,, \tag{B11}$$

with $\mu_9^a < 1$, $\mu_9^b > 1$, $\mu_9^c < 1$. When arbitrary values are assigned to α, β, γ and δ, we can find a ε according to the compatible condition in Eq. (13) as

$$\varepsilon = 2\arctan\frac{(1-\zeta_9)\cdot\tan\dfrac{\alpha+\beta}{2}}{\zeta_9+1}\,,\quad \zeta_9 = \frac{1}{\mu_9^a\cdot\mu_9^b}\,. \tag{B12}$$

Therefore, the type of QRS twist is rigidly foldable once the obtained ε is within the range $(0,\pi)$.

For the QSS twist (Fig. 10(j)), the μ_i^j of this type are

$$\mu_{10}^{a} = \frac{-\cos\dfrac{\alpha+\gamma}{2}}{\cos\dfrac{\alpha-\gamma}{2}}, \quad \mu_{10}^{b} = \frac{\cos\dfrac{\beta+\delta}{2}}{\cos\dfrac{\beta-\delta}{2}}, \quad \mu_{10}^{c} = \frac{\sin\dfrac{\alpha+\beta-\varepsilon}{2}}{\sin\dfrac{\alpha+\beta+\varepsilon}{2}}, \tag{B13}$$

with $\mu_{10}^{a} < 1$, $\mu_{10}^{b} < 1$, $\mu_{10}^{c} < 1$, so it is impossible to find solutions for Eq. (13). Therefore, the type of QSS twist is not rigidly foldable.

For the PSR twist (Fig. 10(k)), the μ_{i}^{j} of this type are

$$\mu_{11}^{a} = \frac{\sin\dfrac{\alpha+\gamma}{2}}{\sin\dfrac{\alpha-\gamma}{2}}, \quad \mu_{11}^{b} = \frac{\cos\dfrac{\beta+\delta}{2}}{\cos\dfrac{\beta-\delta}{2}}, \quad \mu_{11}^{c} = \frac{-\cos\dfrac{\alpha+\beta-\varepsilon}{2}}{\cos\dfrac{\alpha+\beta+\varepsilon}{2}}, \tag{B14}$$

with $\mu_{11}^{a} > 1$, $\mu_{11}^{b} < 1$, $\mu_{11}^{c} > 1$. When arbitrary values are assigned to α, β, γ and δ, we can find a ε according to the compatible condition in Eq. (13) as

$$\varepsilon = 2\arctan\frac{\zeta_{11}+1}{(\zeta_{11}-1)\cdot\tan\dfrac{\alpha+\beta}{2}}, \quad \zeta_{11} = \frac{1}{\mu_{11}^{a}\cdot\mu_{11}^{b}}. \tag{B15}$$

Therefore, the type of PSR twist is rigidly foldable once the obtained ε is within the range $(0,\pi)$.

For the QSR twist (Fig. 10(l)), the μ_{i}^{j} of this type are

$$\mu_{12}^{a} = \frac{-\cos\dfrac{\alpha+\gamma}{2}}{\cos\dfrac{\alpha-\gamma}{2}}, \quad \mu_{12}^{b} = \frac{\cos\dfrac{\beta+\delta}{2}}{\cos\dfrac{\beta-\delta}{2}}, \quad \mu_{12}^{c} = \frac{-\cos\dfrac{\alpha+\beta-\varepsilon}{2}}{\cos\dfrac{\alpha+\beta+\varepsilon}{2}}, \tag{B16}$$

with $\mu_{12}^{a} < 1$, $\mu_{12}^{b} < 1$, $\mu_{12}^{c} > 1$. When arbitrary values are assigned to α, β, γ and δ, we can find a ε according to the compatible condition in Eq. (13) as

$$\varepsilon = 2\arctan\frac{\zeta_{12}+1}{(\zeta_{12}-1)\cdot\tan\dfrac{\alpha+\beta}{2}}, \ \zeta_{12}=\frac{1}{\mu_{12}^{a}\cdot\mu_{12}^{b}}. \tag{B17}$$

Therefore, the type of QSR twist is rigidly foldable once the obtained ε is within the range $(0,\pi)$.

ACKNOWLEDGMENT

FUNDING

REFERENCES

[1] Zirbel, S. A., Lang, R. J., Thomson, M. W., Sigel, D. A., Walkemeyer, P. E., Trease, B. P., Magleby, S. P., and Howell, L. L., 2013, "Accommodating Thickness in Origami-Based Deployable Arrays," Journal of Mechanical Design, 135(11), pp. 111005-111011.

[2] O'Rourke, J., 2011, How to fold it: the mathematics of linkages, origami, and polyhedra, Cambridge University Press.

[3] Miura, K., 1985, "Method of packaging and deployment of large membranes in space," The Institute of Space and Astronautical Science report, 618, pp. 1-9.

[4] Reis, P. M., Jiménez, F. L., and Marthelot, J., 2015, "Transforming architectures inspired by origami," Proceedings of the National Academy of Sciences, 112(40), pp. 12234-12235.

[5] Lee, T.-U., and Gattas, J. M., 2016, "Geometric design and construction of structurally stabilized accordion shelters," Journal of Mechanisms and Robotics, 8(3), p. 031009.

[6] Belke, C. H., and Paik, J., 2017, "Mori: A Modular Origami Robot," IEEE/ASME Transactions on Mechatronics, 22(5), pp. 2153-2164.

[7] Zhakypov, Z., Belke, C., and Paik, J., 2017, "Tribot: A Deployable, Self-Righting and Multi-Locomotive Origami Robot," IEEE International Conference on Intelligent Robots and Systems (IROS), Vancouver, BC, September 24-28.

[8] Kuribayashi, K., Tsuchiya, K., You, Z., Tomus, D., Umemoto, M., Ito, T., and Sasaki, M., 2006, "Self-deployable origami stent grafts as a biomedical application of Ni-rich TiNi shape memory alloy foil," Materials Science and Engineering: A, 419(1), pp. 131-137.

[9] Miyashita, S., Guitron, S., Ludersdorfer, M., Sung, C. R., and Rus, D., "An untethered miniature origami robot that self-folds, walks, swims, and degrades," Proc. 2015 IEEE International Conference on Robotics and Automation (ICRA), pp. 1490-1496.

[10] Miyashita, S., Guitron, S., Yoshida, K., Shuguang, L., Damian, D. D., and Rus, D., "Ingestible, controllable, and degradable origami robot for patching stomach wounds," Proc. 2016 IEEE International Conference on Robotics and Automation (ICRA), pp. 909-916.

[11] Guitron, S., Guha, A., Li, S., and Rus, D., "Autonomous locomotion of a miniature, untethered origami robot using hall effect sensor-based magnetic localization," Proc. 2017 IEEE International Conference on Robotics and Automation (ICRA), pp. 4807-4813.

[12] Evans, T. A., Lang, R. J., Magleby, S. P., and Howell, L. L., 2015, "Rigidly foldable origami twists," Origami, 6, pp. 119-130.

[13] Nojima, T., 2002, "Modelling of folding patterns in flat membranes and cylinders by origami," JSME International Journal Series C Mechanical Systems, Machine Elements and Manufacturing, 45(1), pp. 364-370.

[14] Wu, W., and You, Z., 2010, "Modelling rigid origami with quaternions and dual quaternions," Proceedings of the Royal Society A: Mathematical, Physical and Engineering Science, 466(2119), pp. 2155-2174.

[15] Tachi, T., 2009, "Generalization of rigid-foldable quadrilateral-mesh origami," Journal of the International Association for Shell and Spatial Structures, 50(3), pp. 173-179.

[16] Dai, J. S., and Jones, J. R., 1999, "Mobility in metamorphic mechanisms of foldable/erectable kinds," Journal of Mechanical Design, 121(3), pp. 375-382.

[17] Demaine, E. D. and O'Rourke, J., 2007, Geometric Folding Algorithms: Linkages, Origami, Polyhedra, Cambridge University Press.

[18] Wei, G., and Dai, J. S., 2014, "Origami-inspired integrated planar-spherical overconstrained mechanisms," Journal of Mechanical Design, 136(5), p. 051003.

[19] Zhang, K., Fang, Y., Fang, H., and Dai, J. S., 2010, "Geometry and constraint analysis of the three-spherical kinematic chain based parallel mechanism," Journal of Mechanisms and Robotics, 2(3), p. 031014.

[20] Qiu, C., Zhang, K., and Dai, J. S., 2016, "Repelling-Screw Based Force Analysis of Origami Mechanisms," Journal of Mechanisms and Robotics, 8(3), pp. 031001-031010.

[21] Zhang, K., Qiu, C., and Dai, J. S., 2016, "An Extensible Continuum Robot with Integrated Origami Parallel Modules," Journal of Mechanisms and Robotics, 8(3), pp. 031010-031019.

[22] Salerno, M., Zhang, K., Menciassi, A., and Dai, J. S., 2016, "A Novel 4-DOF Origami Grasper with an SMA-Actuation System for Minimally Invasive Surgery," IEEE Transactions on Robotics, 32(3), pp. 484-498.

[23] Zhang, X., and Chen, Y., 2018, "Mobile assemblies of Bennett linkages from four-crease origami patterns," Proceedings of the Royal Society A: Mathematical, Physical and Engineering Science, 474(2210), p.20170621.

[24] Zhang, K., and Dai, J. S., 2014, "A kirigami-inspired 8R linkage and its evolved overconstrained 6R linkages with the rotational symmetry of order two," Journal of Mechanisms and Robotics, 6(2), p. 021007.

[25] Mitani, J., 2016, 3D Origami Art, CRC Press.

[26] Cipra, B., 1998, "Proving a Link Between Logic and Origami," Science, 279(5352), pp. 804-805.

[27] Denavit, J., and Hartenberg, R. S., 1955, "A kinematic notation for lower-pair mechanisms based on matrices," ASME J. Appl. Mech., pp. 215-221.

[28] Evans, T. A., Lang, R. J., Magleby, S. P., and Howell, L. L., 2015, "Rigidly foldable origami gadgets and tessellations," Royal Society open science, 2(9), p. 150067.

[29] Bricard, R., 1897, Mémoire sur la théorie de l'octaèdre articulé, J. Math. Pures Appl. Liouville, 3, pp. 113–148.

[30] Bricard, R., 1927, Cinématique appliquée, Gauthier-Villars.

[31] Baker, J. E., 1993, "A comparative survey of the Bennett-based, 6-revolute kinematic loops," Mechanism and Machine Theory, 28(1), pp. 83-96.

Table Caption List

Table A1   Classification of M-V assignments for the generalized triangle twist

origami pattern

Figure Captions List

Fig. 1   (a) An art triangle twist, (b) a generalized triangle twist, where α_0, β_0, γ_0, δ_0 and ε_0 is arbitrary within the domain $(0, \pi)$ and $\alpha_0 + \beta_0 \in (0, \pi)$.

Fig. 2   The D-H notation of adjacent links connected by revolute joints

Fig. 3   A spherical 4R linkage

Fig. 4   Four-crease origami vertices with two schemes of M-V assignment, (a) Vertex-I, and (b) Vertex-II.

Fig. 5   The relationship between the kinematic variable and the dihedral angle for (a) the mountain crease, and (b) the valley crease.

Fig. 6   A generalized triangle twist origami pattern with a specific M-V assignment: (a) the general representation, and (b) the simplified one.

Fig. 7   Three types of the triangle twist origami patterns where (a) each crease-pair is intersected, or (b) only one crease-pair is parallel, or (c) each crease-pair is parallel.

Fig. 8   Four types of M-V assignment of one vertex in the generalized triangle twist origami pattern where the minimum angle is (a) α_{12} or α_{23} for Type P, (b) α_{23} or α_{34} for Type Q, (c) α_{34} or α_{41} for Type R, and (d) α_{41} or α_{12} for Type S.

Fig. 9   Duplicated M-V assignments: (a) the M-V assignment obtained by flipping the paper in Fig. A1 No.5, (b) the one obtained by rotating (a)

along the center of the triangle ABC, and (c) the one copied from Fig. A1 No.17.

Fig. 10   Twelve unique schemes of M-V assignment of the generalized triangle twist origami pattern with vertex-types being (a) PPP, (b) PPQ, (c) PQQ, (d) PRR, (e) PRS, (f) PSS, (g)QQQ, (h) QRR, (i) QRS, (j) QSS, (k) PSR and (l) QSR.

Fig. 11   Physical triangle twist models with $\alpha = 55°$, $\beta = 50°$, $\gamma = 50°$, $\delta = 45°$ and $\varepsilon = 35.44°$ for (a) origami pattern, and (b) kirigami pattern.

Fig. 12   Equivalent mechanisms of the generalized triangle twist: (a) the network of three spherical 4R linkages for the origami pattern, and (b) the derived overconstrained 6R linkage for the kirigami pattern.

Fig. 13   Schematic diagrams of the derived overconstrained 6R linkages when (a) $\gamma \neq \delta$, and (b) $\gamma = \delta$.

Fig. 14   Kinematic paths of the derived overconstrained 6R linkages when each crease-pair is intersected with $\alpha = 55°$, $\beta = 50°$, $\gamma = 50°$, $\delta = 45°$, $\varepsilon = 35.44°$ as solid lines and when only one crease-pair is parallel with $\alpha = 55°$, $\beta = 50°$, $\gamma = \delta = 45°$, $\varepsilon = 33.52°$ as dashed lines.

Fig. A1   All possible schemes of M-V assignment of the generalized triangle twist origami pattern: No.1 PPP, No.2 PPQ, No.3 PQP, No.4 PQQ, No.5 PRR, No.6 PRS, No.7 PSR, No.8 PSS, No.9 QPP, No.10 QPQ, No.11 QQP, No.12 QQQ, No.13 QRR, No.14 QRS, No.15 QSR, No.16 QSS, No.17 RPR, No.18 RPS, No.19 RQR, No.20 RQS, No.21 RRP, No.22 RRQ, No.23 RSP, No.24

RSQ, No.25 SPR, No.26 SPS, No.27 SQR, No.28 SQS, No.29 SRP, No.30 SRQ, No.31 SSP, and No.32 SSQ.